Magnetic and electrical transport properties of Ru doped cobalt ferrite thin films with perpendicular magnetic anisotropy

Monalisha Peda, and P. S. Anil Kumar

COLLECTIONS

Paper published as part of the special topic on 65th Annual Conference on Magnetism and Magnetic Materials, 65th Annual Conference on Magnetism and Magnetic Materials, 65th Annual Conference on Magnetism and Magnetic Materials, 65th Annual Conference on Magnetism and Magnetic Materials, 65th Annual Conference on Magnetism and Magnetic Materials and 65th Annual Conference on Magnetism and Magnetic Materials

View Online   Export Citation   CrossMark

ARTICLES YOU MAY BE INTERESTED IN

Enhancement of spin–orbit torque and modulation of Dzyaloshinskii–Moriya interaction in $Pt_{100-x}Cr_x$/Co/AlO_x trilayer
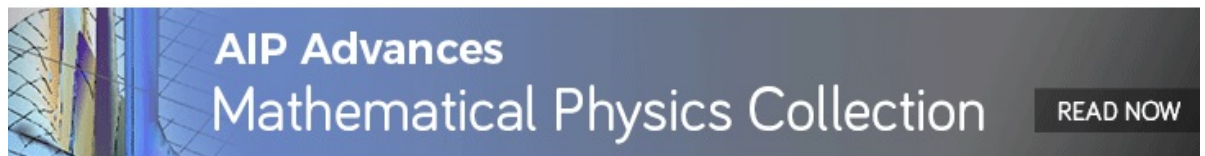Applied Physics Letters **117**, 222405 (2020); https://doi.org/10.1063/5.0030880

Orientation control of optical mode ferromagnetic resonance: From uniaxial to omni-directional
Applied Physics Letters **118**, 022405 (2021); https://doi.org/10.1063/5.0031425

Control of magnetic anisotropy in a Co thin film on a flexible substrate by applying biaxial tensile strain
Applied Physics Letters **118**, 022406 (2021); https://doi.org/10.1063/5.0035003

Magnetic and electrical transport properties of Ru doped cobalt ferrite thin films with perpendicular magnetic anisotropy

View Online   Export Citation   CrossMark

Monalisha Peda (iD) **and P. S. Anil Kumar**[a)]

AFFILIATIONS

Department of Physics, Indian Institute of Science, Bangalore 560012, India

Note: This paper was presented at the 65th Annual Conference on Magnetism and Magnetic Materials.
[a)]**Author to whom correspondence should be addressed:** anil@iisc.ac.in

ABSTRACT

Epitaxial ferrimagnetic thin films of (Co, Ru) Fe_2O_4 were grown on MgO (001) substrate using pulsed laser deposition technique. Ruthenium substitution in cobalt ferrite has increased the conductivity by orders of magnitude, but it has a minimal effect on magnetic properties. The film has a high coercivity and perpendicular magnetic anisotropy (PMA), where the magnetic easy axis points perpendicular to the film surface. We report the magnetic and electrical transport properties here. The temperature variation of resistivity showed different conduction mechanisms at high and low-temperature regimes. Room temperature Hall measurement reveals "n" type carrier with a carrier concentration of $4 \times 10^{20}/cm^3$. The film showed negative MR and a linear decrement with the magnetic field without any saturation.

INTRODUCTION

Room temperature magnetic semiconductors have drawn significant attention due to their potential applications in spin-based spintronic devices such as MRAM,[1,2] ferromagnetic field-effect transistor (FET).[3–5] The metallic ferromagnetic films having PMA are primarily used in ultra-high-density magnetic recording.[6,7] There is a lack of sufficient oxide-based magnetic semiconductors with PMA. Cobalt ferrite (CFO) is a suitable magnetic oxide with combined traits of a tunable magnetic semiconductor and PMA. Cobalt ferrite has an inverse spinel structure, and the metal ions occupy two different sites, namely oxygen tetrahedral (A) and oxygen octahedral (B). The transition metal ion Co^{2+} occupies the B site while an equal number of Fe^{3+} occupy both A and B sites. The insulating nature of cobalt ferrite is due to a lack of hopping conduction at the B site, where all Fe ions exist with a +3 valence state. It has a high Curie temperature (T_c ~860 K) due to antiferromagnetic superexchange interaction between A and B sites. Cobalt ferrite has a high positive first-order magnetocrystalline anisotropy constant accompanied by a considerable value of magnetostriction due

to a large orbital moment of Co^{2+} at the octahedral site.[8] In thin films, the strain related distortion mostly caused by lattice mismatch between film and substrate coupled with high magnetostriction leads to PMA.[9,10] Even though CFO has PMA and essential magnetic properties, the insulating nature of CFO restrict its use in many spintronics application. So, to realize spin-polarized carriers in an oxide-based magnetic semiconductor with PMA, we have substituted Co^{2+} ion with dopants having a valence state more than +3. In this case, it is Ru^{4+}. Ruthenium preferentially occupies the B site with a low spin state.[11] So doping retains its hard-magnetic behavior and PMA while modifying the electrical property significantly. Ru doping results in Fe^{3+}/Fe^{2+} mixed-valence state at B site to maintain charge neutrality. This supports the hopping of spin-polarized 3d-t_{2g} electrons and transforms insulating cobalt ferrite to semiconducting. In this work, we have fabricated a ferromagnetic semiconductor that is a ruthenium doped cobalt ferrite thin film with PMA. We have focused on magnetic, electrical, and magnetotransport properties and tried to understand the primary conduction mechanism. This work demonstrates the potential use of an oxide-based magnetic semiconductor with spin-polarized carriers in spintronics based devices.

EXPERIMENTAL METHODS

We have deposited Ruthenium doped cobalt ferrite ($Co_{0.8}Ru_xFe_2O_4$ - CRFO) thin film using pulsed laser deposition (PLD) technique. The PLD system used a KrF excimer laser (λ=248 nm, 20 ns pulses). The target was prepared by the conventional solid-state reaction method using high-quality precursors Fe_3O_4, RuO_2, Co_3O_4 from Sigma Aldrich. We have used a single-crystalline MgO (001) substrate, which has a lattice mismatch of -0.4 % (tensile). The films were deposited at a frequency of 3 Hz and with an energy fluence of 1.2 J/cm². We have maintained a substrate temperature of 600 °C during the deposition process. The film was *in situ* annealed at 450 °C for 1 hour. We did the film deposition and annealing at a high vacuum of 2× 10^{-5} mbar. The crystal structure and thickness of the film were analyzed using a high-resolution X-Ray diffractometer (Rigaku smartLab). We investigated the surface roughness and magnetic domain structure using an AFM machine. The in-plane (IP) and out-of-Plane (OOP) magnetic hysteresis loops were measured using a superconducting quantum interference device (SQUID, Quantum Design) with a maximum applied field of ± 7 T. We fabricated a Hall bar pattern using a shadow mask during the deposition for transport measurements and carried out the measurements in a four-probe configuration. We performed the electrical and magnetotransport measurements using a physical property measurement system (PPMS, Quantum Design) with a magnetic field applied perpendicular to the film plane.

RESULTS AND DISCUSSION

Fig 1(a) shows the high-resolution 2θ-ω measurement for CRFO/MgO film. The appearance of only the CRFO (004) peak suggests phase-pure growth and the film's highly oriented nature along (*00l*) direction. The out-of-plane lattice constant was calculated from the 2θ position using Bragg's law, giving a value of 8.36 Å. We examined the film's crystallinity quality by performing an omega scan about the CRFO (004) peak. The peak had a minimal FWHM value of $\omega = 0.3°$, shown in Fig 2(b). This shows the highly crystalline nature of the film. We did *in situ* annealing to improve the crystallinity of the film and also to minimize the defects. The thickness of the film was in the range of 40-60 nm. The film's surface morphology and the corresponding MFM image are shown in Fig 1(c) and Fig 1(d), respectively. The surface roughness was measured using the AFM system in a scan area of 2 μm ×2 μm. It showed an rms roughness of as low as 0.2 nm showing an extremely smooth surface. The magnetic microstructure of the film was measured using MFM in the corresponding area. The MFM image was taken in a demagnetized (as prepared sample) state and at room temperature. We have used a magnetic tip coated with Co/Cr thin film at a lift height of 90 nm for MFM measurement. Before measurement, we have magnetized the tip vertically. The MFM image shows domain points in both up and down directions shown by a purple and yellow color, respectively. The magnetic domain image showed a cluster like feature and had different shape and size. The cluster type domain is mostly found in samples with perpendicular anisotropy and with large coercivity.[12]
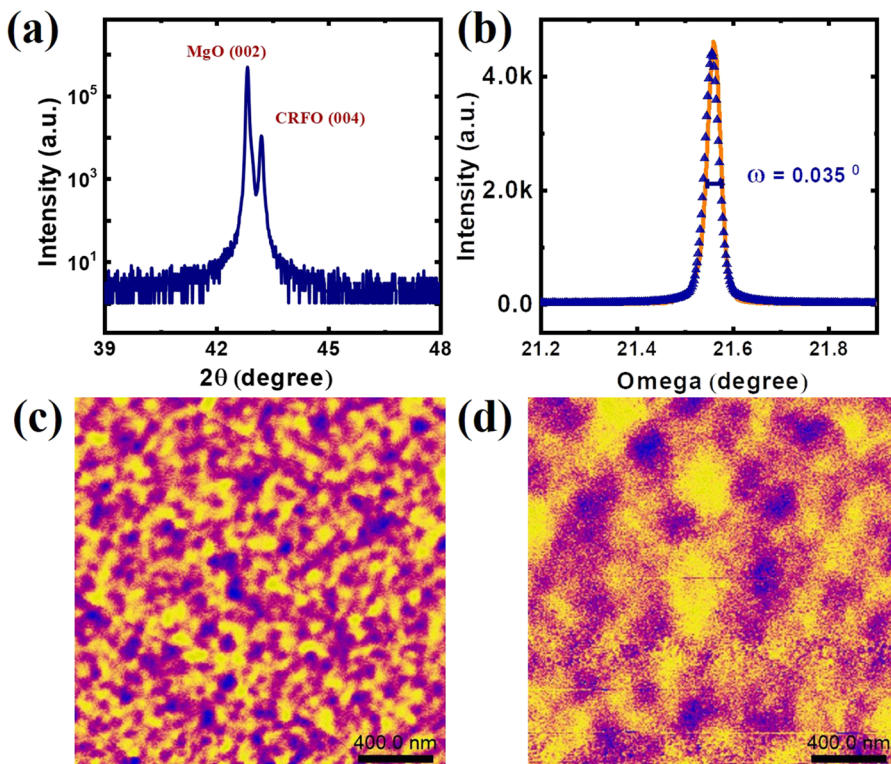

FIG. 1. (a) 2θ-ω measurement shows only (004) peak from CRFO. (b) Omega scan around CRFO (004) peak shows high crystallinity quality of the film with $\omega = 0.03°$ (c) AFM measurement reveals very smooth surface with an rms roughness of 0.2 nm (d) MFM measurement done in remanent state of the film showing cluster like feature.
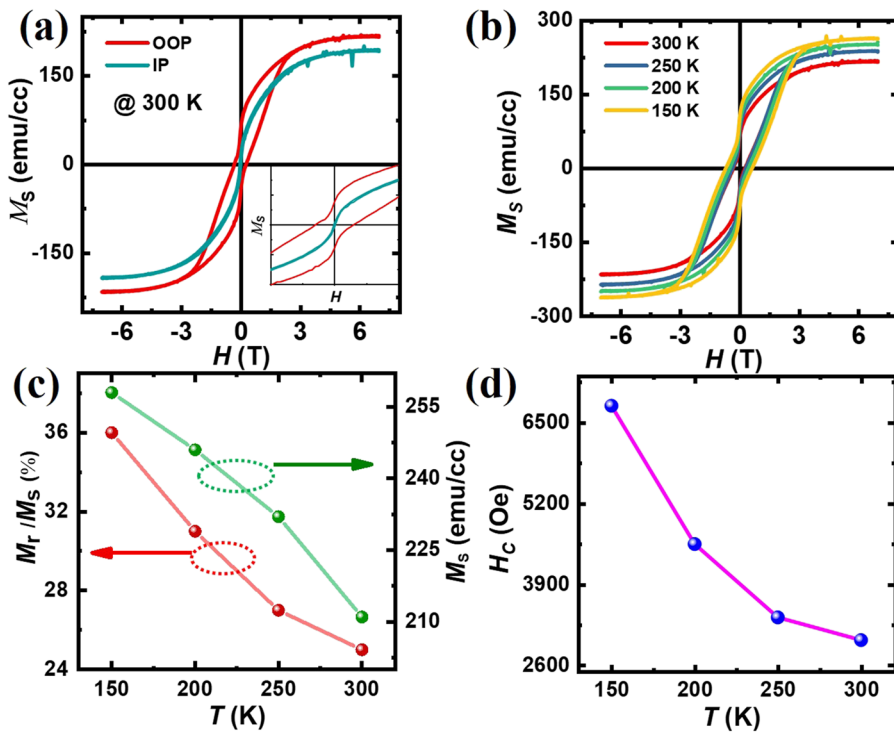
FIG. 2. (a) In-plane and out-of-plane magnetic hysteresis loop measured at room temperature showing OOP is the easy axis, the inset shows the zoomed view at lower magnetic field. (b) OOP M-H loop measured at different temperature. (c) The variation of remanence (M_r/M_s) and saturation magnetization (M_s) with temperature. (d) The variation of OOP coercivity with temperature.

Fig 2(a) shows the room temperature magnetic hysteresis loop of the film in the out-of-plane and in-plane direction. The inset showed the zoomed view of the loop at the lower field. No magnetic remanence in the in-plane M-H loop shows the easy axis of magnetization is perpendicular to the film plane. The CRFO film has undergone tensile strain in an in-plane direction. It leads to high strain anisotropy because of the large negative magnetostriction coefficient of CRFO. As a result of this, the magnetic easy axis lies perpendicular to the film plane. The out-of-plane hysteresis loop has a large value of both saturation magnetization (M_s = 190 emu/cc) and coercivity (H_c = 2000 Oe). M_s values of ruthenium doped cobalt ferrite (CRFO) are comparable to those of cobalt ferrite (CFO) on the MgO substrate.[9,13,14] It is noteworthy to point out that with Ru doping, the film's magnetic properties are slightly affected. The lower value of M_s on MgO substrate was due to the formation of the antiphase boundary (APB). The presence of APB deteriorates the magnetic propertied drastically. In this case, APBs formed due to the high symmetry nature of the MgO substrate than the CRFO film result in many nucleation sites.[15] The OOP M-H loop has a squareness (Mr/Ms) of 35 %. The smaller squareness is due to the presence of in-plane domains and domains with easy axis tilted away from the normal direction in a remanent state.[16] We could notice shrinkage in the M-H loop at the lower field.

We obtained a similar loop for CFO films of thickness ~40 nm on MgO.[17–19] The shrinkage may be arising because while sweeping the field from positive to negative field, there could be nucleation of domain walls due to the presence of an antiphase boundary.[19] We have also studied the temperature dependence of magnetic properties of CRFO thin film. The OOP magnetic hysteresis loop was measured at different temperatures as plotted in Fig 2(b). Fig 2(c)

summarizes the variation of remanence (M_r/M_s) and M_s with temperature. It showed that both remanence and Mr have a higher value at a lower temperature due to perfect spin alignment with reduced thermal agitation. The value decreases as we approach room temperature. The large coercivity of CRFO film is due to the high magnetocrystalline anisotropy constant of Co^{2+} in the octahedral site. The variation of coercivity with temperature is shown in Fig 2(d). It shows that the coercivity decreases rapidly with the increase of temperature. The magnetic anisotropy is usually very sensitive to temperature and has a high value at low temperature. Coercivity variation with temperature reflects temperature dependence of magnetic anisotropy.[20]

Fig 3(a) shows the temperature dependence of electrical resistivity (ρ) of CRFO thin film in a temperature range of 140 - 400 K. The increasing trend of resistivity at lower temperature indicates semiconducting nature. With ruthenium doping, the resistivity of cobalt ferrite has decreased by orders of magnitude. We found that the room temperature resistivity of CRFO film was ~ 2×10^{-1} Ω-cm, while that of CFO had a room temperature resistivity of 10^5 - 10^6 Ω-cm.[21] In CRFO film, Ru^{4+} substitute Co^{2+} and may be preferentially occupying octahedral (B) site due to larger ionic radii.[20,22] It converts Fe^{3+} to Fe^{2+} to maintain charge neutrality and hence increases conduction by hopping of single spin state t_{2g} electrons at B site shown in the inset of Fig 3(a). Adding to Ru doping, the high vacuum growth of CRFO film also facilitated Fe^{3+} to Fe^{2+} conversion due to oxygen deficiency and, hence increasing the conductivity. We examined the doping-induced change in the valence state of Fe using XPS measurement (data are shown in supplementary material). The ρ vs. T data was fitted to different models to understand the underlying conduction mechanism. In Fig 3(b), We
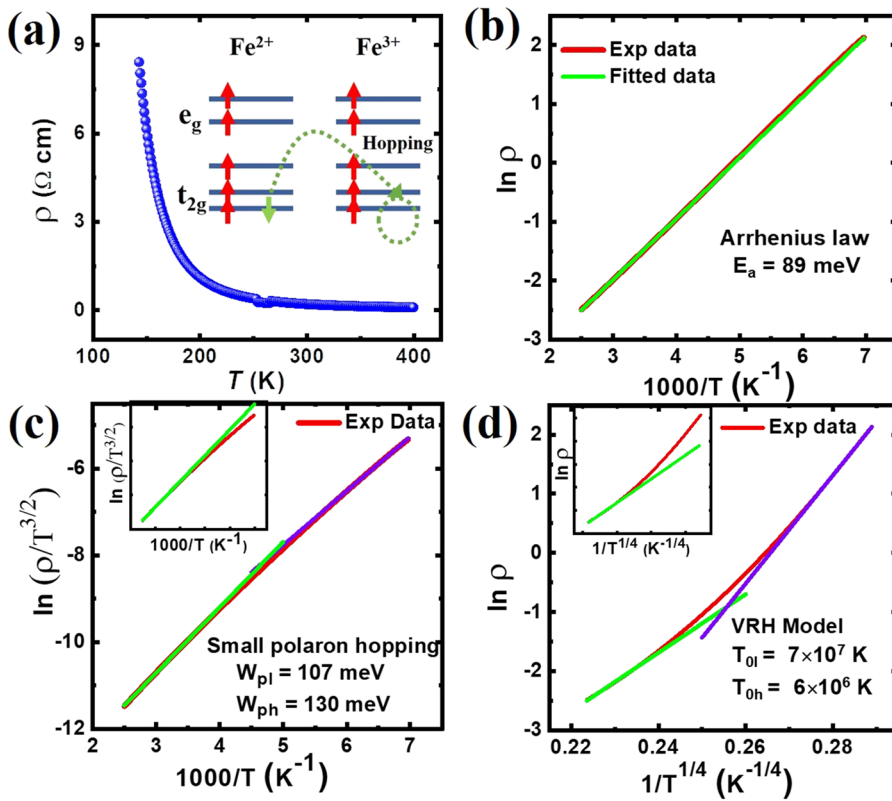
FIG. 3. (a) The temperature variation of resistivity for CRFO thin film. (b) Fitted with Arrhenius formula from 140 K to 400 K, indicating E_a = 89 meV. (c) Fitting with small polaron hopping model with double slope giving W_{pl} =107 meV and W_{ph} =130 meV, inset shows fitting to a single slope. (d) Fitting with variable range hopping model with double slope giving T_{0l}= 7×10^7 K and T_{0h}= 6×10^6 K, the inset shows fitting with a single slope.

fitted the data to Arrhenius type equation defined as

$$\rho_{xx} = \rho_0 \exp(E_a/K_B T) \qquad (1)$$

where ρ_0, E_a, K_B is a preexponential constant, activation energy for allowing hopping of electron from Fe^{2+} to Fe^{3+} and the Boltzmann constant, respectively. From the slope of $\ln \rho$ vs. 1000/T graph, we found the E_a value to be 89 meV.[23] The Arrhenius plot showed good linearity throughout the temperature range of 140 - 400 K, giving clear evidence of thermally activated conduction.[24,25] The electron conduction in some other spinel ferrites were explained by the small polaron hopping model[26,27] Which is defined as

$$\rho_{xx} = \rho_0 T^{3/2} \exp(W_P/K_B T) \qquad (2)$$

where ρ_0, w_p, K_B are preexponential term, potential barrier for hopping, and Boltzmann constant, respectively.[26] Fig 3(c) shows $\ln(\rho/T^{3/2})$ vs. 1000/T graph was fitted to two lines (of a different slope) at low (140-210 K) and high (210-400 K)-temperature range despite one line in the whole temperature range. Fitting to a single line shows discrepancy at a lower temperature, as shown in the inset of Fig 3(c). This reflects a change in the conduction mechanism at ~ 210 K. We obtained the fitting parameter W_{PL} = 107 meV and W_{PH} = 130 meV corresponding to low and high temperature, respectively.[26,28] It was also possible to fit the data by assuming Mott's variable range hopping (VRH) in the whole temperature range, as shown in Fig 3(d). The equation was defined as

$$\rho_{xx} = \rho_0 \exp(T_0/T)^{1/4} \qquad (3)$$

Where T_0 is the mott characteristic temperature.[29] Again, the fitting resulted in two slopes with values of T_{0L} =7×10^{-7} K and T_{0H} = 6×10^{-6} K at the low (140-233 K) and high (233-400 K) temperature range, respectively.[23,30] The inset shows a bad fitting at a lower temperature when fitted with a single line.

Fitting with various models, we found that the transport mechanism of the magnetic semiconductor is well understood using the small polaron hopping model and Mott's variable range hopping (VRH). There is a cross-point temperature in the range of 210 K - 233 K, where a change of conduction mechanism occurs. The carriers have a thermally activated behavior with two activation energy below and above this temperature. This temperature dependence ρ with two activation energies resembles the other spinel ferrite thin films.[30] This double activation energy is due to defects associated with the film.[31]

In Fig 4(a-d), we have demonstrated the magnetotransport properties to investigate the intriguing magnetic properties of the magnetic semiconductor. Fig 4(a) showed the schematic illustration of the Hall bar device used for electric and magnetic transport measurements. The magnetic field was applied perpendicular to the film plane. In a ferromagnetic material, the hall resistivity is defined by an empirical relation defined as

$$\rho_{xy} = R_0 \mu_0 H + R_A \mu_0 M \qquad (4)$$

The first term in Eq. (4) represents the ordinary Hall effect with R_0 as the normal Hall coefficient. This results from the magnetic Lorentz force. The second term represents the anomalous Hall effect
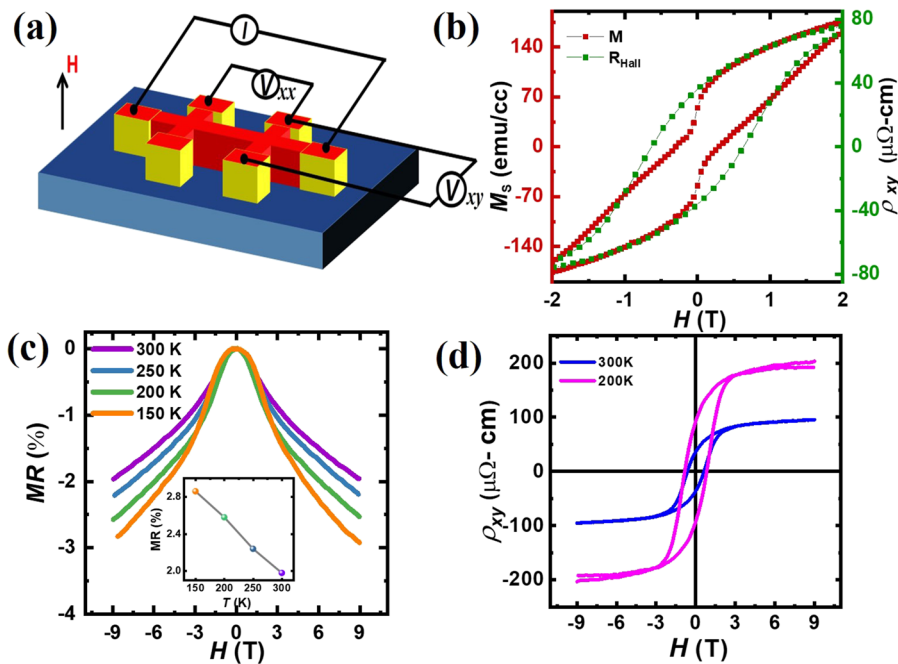
FIG. 4. (a) Schematic illustration of the hall bar device with electrical connections for transport measurements. (b) Overlapping of ρ_{xy} and OOP M-H loop at lower field showing presence of AHE at room temperature. (c) Magnetoresistance measurement at different temperature (d) MR Variation with temperature.

(AHE), and it depends on the perpendicular magnetization of the sample with R_A as the anomalous Hall coefficient. Usually, AHE has a more considerable contribution than the ordinary Hall effect. The room temperature variation of Hall resistivity and out-of-plane magnetization with the magnetic field is shown in Fig 4(b). The loops overlapped at lower field values ($H < 2\,T$) confirms the occurrence of AHE. AHE at room temperature signifies the presence of spin-polarized carriers. Fig 4(d) present ρ_{xy} variation with the magnetic field at 300 K and at 200 K. R_A value calculated to be 3.06 ×10⁻⁷ m^3/As and 6.7 ×10⁻⁷ m^3/As at 300 K and 200 K, respectively. It shows an increment of spin polarization at low temperatures. From Hall measurement, we found the carrier type to be "n" type with a carrier concentration of 4.4 ×10²⁰/cm³ and 2.7 ×10²⁰/cm³ and mobility of 0.23 cm²/Vs and 0.06 cm²/Vs at 300 K and 200 K, respectively. This implies that both carrier concentration and mobility have lower values at a lower temperature.[23]

We measured the change in resistance with the magnetic field, magnetoresistance (MR) of the CRFO film with magnetic field variation. The highest applied field was up to ± 9 T in the perpendicular direction.

The MR is defined here as

$$MR = [R(H) - R(0)]/R(0) \qquad (5)$$

Where $R(H)$ and $R(0)$ are the resistance in the presence and absence of a magnetic field, respectively. The MR has a negative value and showed a linear decrement with a magnetic field without saturation. A negative MR arises from defects created in the film during the growth process like APB, stacking defects.[32,33] The APBs couple antiferromagnetically with the adjacent domains. The presence of magnetic field forces parallel alignment of domains results in increased conductance and a negative MR.[34] The MR value was measured at different temperatures, as shown in Fig 4(c). The MR % increased

systematically towards the lower temperature and had the highest value of 2.8 % at 150 K, shown in the inset of Fig 4(c).[35] This may be due to temperature dependence of tunneling of spin-polarized electrons across APBs.[36,37]

CONCLUSION

We have successfully fabricated ferrimagnetic semiconductor, ruthenium doped cobalt ferrite thin film by PLD. The film has high crystallinity and a smooth surface. Ruthenium doping has transformed insulating cobalt ferrite into a magnetic semiconductor without much affecting its magnetic properties. CRFO/MgO has perpendicular magnetic anisotropy produced by stress anisotropy. The M_r/M_s and H_c have a higher value at a lower temperature, and the value decreases as we approach room temperature. We investigated the activated conduction mechanism in the entire temperature range. The AHE demonstrates spin-polarized carriers at room temperature, and it increases at a lower temperature. It also showed a negative MR with the highest value of 2.8 % at 150 K. This shows the potential of our system for spintronics applications.

SUPPLEMENTARY MATERIAL

See supplementary material for the conversion of Fe^{3+} to Fe^{2+} with ruthenium doping without altering the valence state of cobalt.

ACKNOWLEDGMENTS

DATA AVAILABILITY

The data that support the findings of this study are available from the corresponding author upon reasonable request.

REFERENCES

[1] W. Kim, K. Kawaguchi, N. Koshizaki, M. Sohma, and T. Matsumoto, J. Appl. Phys. **93**, 8032 (2003).

[2] X. W. Li, A. Gupta, G. Xiao, W. Qian, and V. P. Dravid, Appl. Phys. Lett. **73**, 3282 (1998).

[3] D. Chiba, M. Yamanouchi, F. Matsukura, and H. Ohno, Science **301**, 943 (2003).

[4] H. Ohno, D. Chiba, F. Matsukura, T. Omiya, E. Abe, T. Dietl, Y. Ohno, and K. Ohtani, Nature **408**, 944 (2000).

[5] T. Kanki, Y.-G. Park, H. Tanaka, and T. Kawai, Appl. Phys. Lett. **83**, 4860 (2003).

[6] Q. Dai, D. Berman, K. Virwani, J. Frommer, P.-O. Jubert, M. Lam, T. Topuria, W. Imaino, and A. Nelson, Nano Lett. **10**, 3216 (2010).

[7] R. Sbiaa, H. Meng, and S. N. Piramanayagam, Phys. Status Solidi – Rapid Res. Lett. **5**, 413 (2011).

[8] Y. Suzuki, G. Hu, R. B. van Dover, and R. J. Cava, J. Magn. Magn. Mater. **191**, 1 (1999).

[9] A. Lisfi, C. M. Williams, L. T. Nguyen, J. C. Lodder, A. Coleman, H. Corcoran, A. Johnson, P. Chang, A. Kumar, and W. Morgan, Phys. Rev. B **76**, 054405 (2007).

[10] J. Inoue, H. Itoh, M. A. Tanaka, K. Mibu, H. Niizeki, H. Yanagihara, and E. Kita, IEEE Trans. Magn. **49**, 3269 (2013).

[11] A. You, M. A. Y. Be, and I. In **2**, 182505 (2015).

[12] A. Hubert and R. Schafer, *Magnetic Domains* (1998).

[13] S. A. Chambers, R. F. C. Farrow, S. Maat, M. F. Toney, and L. Folks, J. Magn. Magn. Mater. **246**, 124 (2002).

[14] J. A. Phys., 113924 (2011).

[15] A. V. Folks, B. Khodadadi, J. B. Mohammadi, S. Keshavarz, T. Mewes, D. S. Negi, R. Datta, Z. Galazka, R. Uecker, and A. Gupta, Adv. Mater. **29**, 1 (2017).

[16] H. Yanagihara, K. Uwabo, M. Minagawa, E. Kita, and N. Hirota, J. Appl. Phys. **109**, 07C122 (2011).

[17] M. Khodaei, S. A. Seyyed Ebrahimi, Y. J. Park, S. H. Choi, C. Kim, J. Son, and S. Baik, Thin Solid Films **571**, 62 (2014).

[18] D. T. Margulies, F. T. Parker, M. L. Rudee, F. E. Spada, J. N. Chapman, P. R. Aitchison, and A. E. Berkowitz, Phys. Rev. Lett. **79**, 5162 (1997).

[19] R. Comes, M. Gu, M. Khokhlov, J. Lu, and S. A. Wolf, J. Magn. Magn. Mater. **324**, 524 (2012).

[20] B. Krutzsch and S. Kemmler-Sack, Mater. Res. Bull. **19**, 1659 (1984).

[21] P. D. Thang, G. Rijnders, and D. H. A. Blank, J. Magn. Magn. Mater. **310**, 2621 (2007).

[22] T. Kanki, Y. Hotta, N. Asakawa, M. Seki, H. Tabata, and T. Kawai, Appl. Phys. Lett. **92**, 182505 (2008).

[23] F. Iwamoto, M. Seki, and H. Tabata, J. Appl. Phys. **112**, 103901 (2012).

[24] Y. F. Chen, D. Spoddig, and M. Ziese, J. Phys. D. Appl. Phys. **41**, 205004 (2008).

[25] D. Venkateshvaran, M. Althammer, A. Nielsen, S. Geprägs, M. S. Ramachandra Rao, S. T. B. Goennenwein, M. Opel, and R. Gross, Phys. Rev. B **79**, 134405 (2009).

[26] R. Ramos, S. K. Arora, and I. V. Shvets, Phys. Rev. B **78**, 214402 (2008).

[27] S. K. Arora, R. G. S. Sofin, I. V. Shvets, R. Kumar, M. W. Khan, and J. P. Srivastava, J. Appl. Phys. **97**, 10C310 (2005).

[28] M. Seki, H. Tabata, H. Ohta, K. Inaba, and S. Kobayashi, Appl. Phys. Lett. **99**, 242504 (2011).

[29] N. F. Mott, J. Non. Cryst. Solids **1**, 1 (1968).

[30] K. Brachwitz, T. Böntgen, M. Lorenz, and M. Grundmann, Appl. Phys. Lett. **102**, 172104 (2013).

[31] Q. Ke, X. Lou, Y. Wang, and J. Wang, Phys. Rev. B **82**, 024102 (2010).

[32] W. Eerenstein, T. T. M. Palstra, S. S. Saxena, and T. Hibma, Phys. Rev. Lett. **88**, 247204 (2002).

[33] T. Hibma, F. C. Voogt, L. Niesen, P. A. A. Van Der Heijden, W. J. M. De Jonge, J. J. T. M. Donkers, and P. J. Van Der Zaag, J. Appl. Phys. **85**, 5291 (1999).

[34] K. Fujiwara, T. Ichimura, and H. Tanaka, Adv. Mater. Interfaces **1**, 1300108 (2014).

[35] D. Tripathy, A. O. Adeyeye, C. B. Boothroyd, and S. N. Piramanayagam, J. Appl. Phys. **101**, 013904 (2007).

[36] D. Tripathy, A. O. Adeyeye, C. B. Boothroyd, and S. Shannigrahi, J. Appl. Phys. **103**, 07F701 (2008).

[37] N. Jedrecy, C. Hebert, J. Perriere, M. Nistor, and E. Millon, J. Appl. Phys. **116**, 213903 (2014).